Engineering Transactions, **68**(3): 239–252, 2020, doi: 10.24423/EngTrans.960.20200720
Polish Academy of Sciences • Institute of Fundamental Technological Research (IPPT PAN)
Université de Lorraine • Poznan University of Technology

Research Paper

Thermodynamics Analysis of an MHD Casson Fluid Flow Through a Rotating Permeable Channel with Slip and Hall Effects

Adetayo Samuel EEGUNJOBI[1)*], Oluwole Daniel MAKINDE[2)]

[1)] *Department of Mathematics and Statistics*
Namibia University of Science and Technology
Private Bag 13388, 13 Storch Street, Windhoek, Namibia
*Corresponding Author e-mail: samdet1@yahoo.com

[2)] *Faculty of Military Science*
Stellenbosch University
Private Bag X2, Saldanha 7395, South Africa

In this paper, the inherent irreversibility in a Casson fluid flow through a rotating permeable microchannel with wall slip and Hall current is investigated. It is assumed that the lower wall is subjected to the velocity slip and fluid injection while the fluid suction occurs at the upper wall. The nonlinear governing equations of momentum and energy balance are obtained, analyzed and solved numerically using the shooting technique together with the Runge-Kutta-Fehlberg integration method. Pertinent results depicting the effects of various embedded thermophysical parameters on the fluid velocity, temperature, skin friction, the Nusselt number, entropy generation rate and the Bejan number are presented graphically and discussed. It is found that the entropy generation rate is enhanced by fluid rotation and velocity slip but lessened with a rise magnetic field intensity. Our results will undoubtedly augment the design and efficient operation of micro-cooling devices, micro-heat exchangers, micropumps and micro-mixing technologies.

Key words: MHD; Casson fluid; rotating flow; permeable channel; Hall effects; entropy analysis.

1. Introduction

Studies related to non-Newtonian fluid flows and heat transfer have attracted the attention of many researchers in recent years because of their wide applications in various fields such as crude oil extraction from petroleum products, processing of food stuffs, production of paper and fiber coating. The versatility characteristics of non-Newtonian fluids make their constitutive equations nonlin-

ear and non-uniform. Therefore, several models have been developed to describe their characteristics. Among them is the Casson model that was introduced by Casson [1] to predict the flow characteristics of pigment oil suspensions of the printing ink type. Casson fluid isassumed to have a zero and infinite viscosity for an infinite and zero rate of shear, respectively, and have a yield stress below which no flow occurs. Many researchers have focused their research on Casson fluid flow due to its wide applications in mechanical and chemical engineering. Gireesha *et al.* [2] investigated heat and mass transfer on a double-diffusive three-dimensional hydromagnetic boundary layer flow of an electrically conducting Casson nanofluid over a stretching surface. Zaib *et al.* [3] used a modified Arrhenius function to examine the influence of second law analysis for an electrically conducting fluid of a Casson nanofluid over a wedge. Gupta and Sharma [4] applied the convective surface boundary conditions together with radiation effects to analyze the magnetohydrodynamic (MHD) three-dimensional flow of Casson nanofluid over a stretching sheet in the presence of thermophoresis and Brownian motion effects. Durairaj *et al.* [5] carried out the study of unsteady, heat-generating/absorbing and chemically reacting Casson fluid flow over a vertical cone and flat plate saturated with the non-Darcy porous medium in the presence of cross-diffusion effects. Hymavathi and Sridhar [6] used the Keller box method to investigate the effect of the mass transfer of an MHD Casson fluid over a porous stretching sheet in the presence of chemical reaction. Hussanan *et al.* [7] tried to establish the exact solutions for the unsteady MHD flow of a Casson fluid over a vertical plate oscillating in its plane taking into consideration the Newtonian heating conditions. Rawi *et al.* [8] investigated the influence of nanoparticles on the unsteady mixed convection flow of Casson fluid past an inclined stretching sheet.

Fluid motion affected by rotation is basically different from non-rotating ones. In the structure and variation of large-scale flows, rotation plays a vital role. Rotating fluid has various applications in geophysics and astrophysics, and it has attracted the interest of many applied mathematicians. Eegunjobi and Makinde [9] investigated inherent irreversibility in a variable viscosity Hartmann flow through a rotating permeable channel with Hall effects. Singh *et al.* [10] presented an analytical study on an unsteady MHD boundary layer flow of a rotating viscoelastic fluid over an infinite vertical porous plate embedded in a uniform porous medium with oscillating free-stream taking into consideration Hall and ion-slip currents. Rashidi and Erfani [11] used the differential transform method and the Padé approximants method to analyze the thermal-diffusion and diffusion-thermo effects on combined heat and mass transfer of a steady MHD convective and slip flow due to a rotating disk with viscous dissipation and Ohmic heating. Papa *et al.* [12] carried out a computational study of laminar flow through a rotating duct with parallel rotation at the outlet.

Arikoglu and Ozkol [13] studied steady MHD flow of a viscous, Newtonian and electrically conducting fluid over a rotating infinite disk with slip boundary condition.

In the existing literature, studies on the combined effects of the magnetic field, Hall current, suction and injection, Joule heating, velocity slip and viscous dissipation on Casson fluid with heat transfer and entropy generation rate in a low aspect ratio permeable and rotating microchannel has not been reported. The main objective of this present study is to fill this information gap. Moreover, this study is very crucial for innovative applications in the design and efficient operation of micro-cooling devices, micro-heat exchangers, micro-pumps and micro-mixing technologies. This paper will carry our exergy analysis of an MHD Casson fluid flow through a rotating permeable channel with slip and Hall Effects. The governing equations are obtained and solved numerically. Pertinent results are presented and discussed.

2. The model problem

Let us consider the steady flow of an incompressible, electrically and thermally conducting Casson fluid across the space separated by two infinite parallel permeable walls $y = 0$ and $y = L$ under the action of an externally imposed transverse magnetic field B_0 and taking into account Hall current. The fluid and channel rotate simultaneously with a monotonous angular velocity Ω about the y-axis. The flow of the fluid inside the channel is induced due to the mutual effects of uniform pressure gradient applied along the x-direction and the suction/injection at the channel walls. The channel lower wall is retained at temperature T_0 while the upper wall is kept at temperature T_1 such that $T_0 < T_1$. A physical model of the problem is presented in Fig. 1. Since channel walls are infinite in the x- and z-directions, the flow is fully developed and all physical

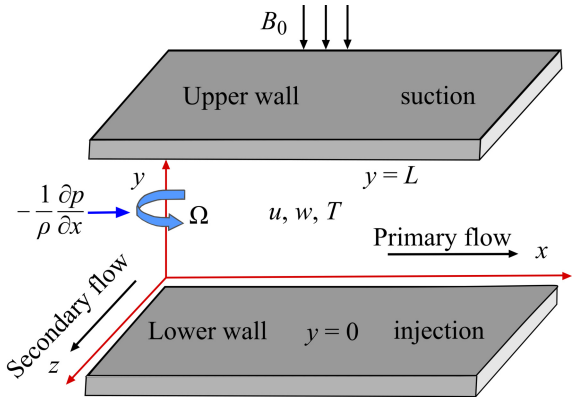

Fig. 1. Physical model of the problem.

quantities, except pressure, depend on y only. The rheological equation of state for an isotropic flow of a Casson fluid can be expressed as [1]

$$\tau_{ij} = \begin{cases} \left(\mu_B + \dfrac{P_y}{\sqrt{2\pi}}\right) 2e_{ij}, & \pi > \pi_c, \\ \left(\mu_B + \dfrac{P_y}{\sqrt{2\pi_c}}\right) 2e_{ij}, & \pi < \pi_c. \end{cases} \tag{2.1}$$

In the above equation, $P_y = e_{ij}e_{ij}$ and e_{ij} denotes the (i, j)-th component of the deformation rate, π is the product of the component of deformation rate with itself, π_c is a critical value of this product based on the non-Newtonian model, μ_B is the plastic dynamic viscosity of the non-Newtonian fluid, and P_y is the yield stress of the fluid. From Eq. (2.1) we obtain (for $\pi < \pi_c$),

$$\tau_{ij} = \mu_B \left(1 + \frac{1}{\beta}\right) 2e_{ij}, \tag{2.2}$$

where $\beta = \mu\sqrt{2\pi_c}/P_y$ is the Casson fluid parameter. It is very important to note that the fluid behavior becomes that of Newtonian fluid as $\beta \to \infty$.

Bearing in mind the assumptions presented above, the governing equations for a steady flow of viscous, incompressible, electrically and thermally conducting fluid in a rotating system coupled with Hall current are presented in the following form:

$$-V\frac{\partial u}{\partial y} + 2\Omega w = -\frac{1}{\rho}\frac{\partial p}{\partial x} + \left(1 + \frac{1}{\beta}\right)\frac{\mu}{\rho}\frac{\partial^2 u}{\partial y^2} - \frac{\sigma B_0^2\,(u + mw)}{\rho(1 + m^2)}, \tag{2.3}$$

$$-V\frac{\partial w}{\partial y} - 2\Omega u = \left(1 + \frac{1}{\beta}\right)\frac{\mu}{\rho}\frac{\partial^2 w}{\partial y^2} - \frac{\sigma B_0^2\,(w - mu)}{\rho(1 + m^2)}, \tag{2.4}$$

$$\frac{k}{\rho c_p}\frac{\partial^2 T}{\partial y^2} + V\frac{\partial T}{\partial y} + \left(1 + \frac{1}{\beta}\right)\frac{\mu}{\rho c_p}\left[\left(\frac{\partial u}{\partial y}\right)^2 + \left(\frac{\partial w}{\partial y}\right)^2\right] - \frac{\sigma B_0^2}{\rho c_p}\left[\frac{(u + mw)^2 + (w - mu)^2}{(1 + m^2)^2}\right] = 0, \tag{2.5}$$

$$E_g = \frac{k}{T_0^2}\left(\frac{\partial T}{\partial y}\right)^2 + \left(1 + \frac{1}{\beta}\right)\frac{\mu}{T_0}\left[\left(\frac{\partial u}{\partial y}\right)^2 + \left(\frac{\partial w}{\partial y}\right)^2\right] + \frac{\sigma B_0^2}{T_0}\left[\frac{(u + mw)^2 + (w - mu)^2}{(1 + m^2)^2}\right], \tag{2.6}$$

where $u, w, T, \sigma, \rho, m = \omega_e\tau_e, \omega_e, \tau_e, k, c_p, E_g, V$, and μ are respectively, the fluid velocity in the x-direction, fluid velocity in the z-direction, fluid temperature, fluid electrical conductivity, fluid density, Hall current parameter, cyclotron frequency, electron collision time, thermal conductivity coefficient, specific heat at constant pressure, the volumetric entropy generation rate, the injection/suction velocity and the fluid dynamic viscosity at larger Casson parameter. The boundary conditions for the fluid velocities and temperature are given as

$$\begin{gathered} u(0) = \left(1 + \frac{1}{\beta}\right) \frac{\mu}{C} \frac{\partial u}{\partial y}(0), \\ w(0) = 0, \quad T(0) = T_0, \quad u(L) = 0, \quad w(L) = 0, \quad T(L) = T_1, \end{gathered} \tag{2.7}$$

where C is the slip length parameter. The dimensionless variables and parameters are as follows:

$$\begin{gathered} \eta = \frac{y}{L}, \quad X = \frac{x}{L}, \quad \theta = \frac{T - T_0}{T_1 - T_0}, \quad \upsilon = \frac{\mu}{\rho}, \quad U = \frac{uL}{\upsilon}, \quad W = \frac{wL}{\upsilon}, \\ \mathrm{Pr} = \frac{\mu c_p}{k}, \quad A = -\frac{\partial \overline{P}}{\partial X}, \quad \gamma = \frac{T_1 - T_0}{T_0}, \quad \mathrm{Ec} = \frac{\upsilon^2}{c_p(T_1 - T_0)L^2}, \\ M = \frac{\sigma B_0^2 L^2}{\mu}, \quad \mathrm{Ro} = \frac{\Omega L^2}{\upsilon}, \quad \mathrm{Ns} = \frac{E_g T_0^2 L^2}{k(T_1 - T_0)^2}, \\ \overline{P} = \frac{L^2 P}{\rho \upsilon^2}, \quad \mathrm{Re} = \frac{VL}{\upsilon}, \quad \delta = \frac{\mu}{CL}. \end{gathered} \tag{2.8}$$

By substituting Eq. (2.8) into Eqs (2.3)–(2.7), we obtain:

$$-\mathrm{Re}\frac{\mathrm{d}U}{\mathrm{d}\eta} + 2\mathrm{Ro}W = A + \left(1 + \frac{1}{\beta}\right) \frac{\mathrm{d}^2 U}{\mathrm{d}\eta^2} - \frac{M(U + mW)}{(1 + m^2)}, \tag{2.9}$$

$$-\mathrm{Re}\frac{\mathrm{d}W}{\mathrm{d}\eta} - 2\mathrm{Ro}U = \left(1 + \frac{1}{\beta}\right) \frac{\mathrm{d}^2 W}{\mathrm{d}\eta^2} - \frac{M(W - mU)}{(1 + m^2)}, \tag{2.10}$$

$$\begin{aligned} \frac{d^2\theta}{\mathrm{d}\eta^2} + \mathrm{Re}\,\mathrm{Pr}\,\frac{\mathrm{d}\theta}{\mathrm{d}\eta} + \mathrm{Pr}\,\mathrm{Ec}\left(1 + \frac{1}{\beta}\right)\left[\left(\frac{\mathrm{d}U}{\mathrm{d}\eta}\right)^2 + \left(\frac{\mathrm{d}W}{\mathrm{d}\eta}\right)^2\right] \\ + \mathrm{Pr}\,\mathrm{Ec}\,M\left[\frac{(U + mW)^2 + (W - mU)^2}{(1 + m^2)^2}\right] = 0, \end{aligned} \tag{2.11}$$

$$\text{Ns} = \left(\frac{\mathrm{d}\theta}{\mathrm{d}\eta}\right)^2 + \frac{\text{Pr Ec}}{\gamma}\left(1+\frac{1}{\beta}\right)\left[\left(\frac{\mathrm{d}U}{\mathrm{d}\eta}\right)^2 + \left(\frac{\mathrm{d}W}{\mathrm{d}\eta}\right)^2\right] + \frac{\text{Pr Ec}M}{\gamma}\left[\frac{(U+mW)^2+(W-mU)^2}{(1+m^2)^2}\right], \tag{2.12}$$

with

$$U(0) = \delta\left(1+\frac{1}{\beta}\right)\frac{\mathrm{d}U}{\mathrm{d}\eta}(0), \quad W(0)=0, \quad \theta(0)=0, \qquad U(1)=0, \quad W(1)=0, \quad \theta(1)=1, \tag{2.13}$$

where Pr is the Prandtl number, Ro is the rotation parameter, Re is the suction Reynolds number, Ec is the Eckert number, δ is the slip parameter, M is the magnetic field parameter, γ is the temperature difference parameter, and A represents the pressure gradient parameter. Other quantities of interest are the skin friction coefficients (Cf_1 and Cf_2), the Nusselt number (Nu) and the Bejan number (Be), which are given as

$$Cf_1 = \frac{L^2\tau_1}{\rho\upsilon^2} = \left(1+\frac{1}{\beta}\right)\left.\frac{\mathrm{d}U}{\mathrm{d}\eta}\right|_{\eta=0,1}, \quad Cf_2 = \frac{L^2\tau_2}{\rho\upsilon^2} = \left(1+\frac{1}{\beta}\right)\left.\frac{\mathrm{d}W}{\mathrm{d}\eta}\right|_{\eta=0,1},$$
$$\text{Nu} = -\frac{Lq_m}{k(T_1-T_0)} = -\left.\frac{\mathrm{d}\theta}{\mathrm{d}\eta}\right|_{\eta=0,1}, \quad \text{Be} = \frac{N_1}{\text{Ns}} = \frac{1}{1+\phi}, \tag{2.14}$$

where

$$\tau_1 = \mu\left(1+\frac{1}{\beta}\right)\frac{\partial u}{\partial y}, \qquad \tau_2 = \mu\left(1+\frac{1}{\beta}\right)\frac{\partial W}{\partial y},$$
$$q_m = -k\frac{\partial T}{\partial y}, \qquad \phi = \frac{N_2}{N_1}, \qquad N_1 = \left(\frac{\mathrm{d}\theta}{\mathrm{d}\eta}\right)^2,$$
$$N_2 = \frac{\text{Pr Ec}}{\gamma}\left(1+\frac{1}{\beta}\right)\left[\left(\frac{\mathrm{d}U}{\mathrm{d}\eta}\right)^2 + \left(\frac{\mathrm{d}W}{\mathrm{d}\eta}\right)^2\right] + \frac{\text{Pr Ec}\,M}{\gamma}\left[\frac{(U+mW)^2+(W-mU)^2}{(1+m^2)^2}\right]. \tag{2.15}$$

It is very crucial to note that N_1 represents the thermodynamic irreversibility due to heat transfer, while N_2 corresponds to the mutual effects of fluid friction and magnetic field irreversibility. When Be = 0.5, both N_1 and N_2 contribute

equally to the entropy generation in the flow process. The model Eqs (2.9)–(2.13) are solved numerically using a shooting technique coupled with the Runge-Kutta-Fehlberg integration scheme. The approach involved converts the model boundary value problem (BVP) into the initial value problem (IVP) and uses the shooting method to get the unknown initial values while the Runge-Kutta-Fehlberg integration scheme is deployed for the solution up to the prescribed boundary conditions.

3. Results and discussion

The graphical representation of the results is very important to establish the influences of various parameters on the entire flow field. Figures 2–4 demonstrate the influences of various parameters on the velocity profile in the x-direction. As shown in Fig. 2, as the slip parameter increases, the thickness of the boundary layer decreases along the lower wall, thereby accelerating fluid transfer successively and causing the velocity profile to rise. It is also seen in Fig. 2 that pressure gradient increment decreases the boundary layer thickness at the lower wall and therefore leads to an increase in the velocity profile. The effects of Hall current and Casson fluid parameters are depicted in Fig. 3. We observe that as these parameters are increasing, the boundary layer decreases, causing an increase in the velocity profile. Meanwhile, the impacts of the magnetic field and rotation parameters are illustrated in Fig. 3. An increase in these parameters leads to a decrease in the velocity profile. This happened because an increase in the magnetic field parameter and Casson fluid parameter caused the boundary layer thickness to increase, therefore decreasing the velocity profile.

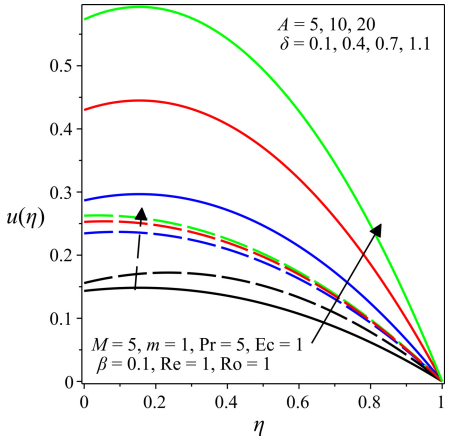

Fig. 2. Velocity profile in the x-direction with varied A and δ.

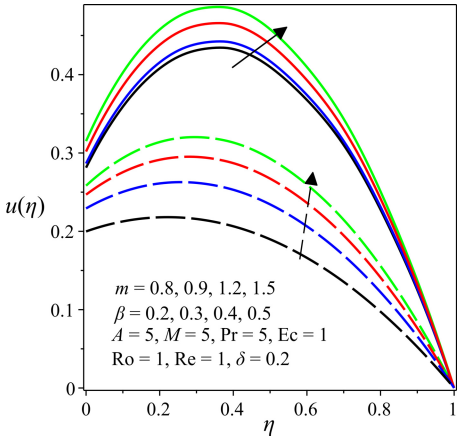

Fig. 3. Velocity profile in the x-direction with varied m and β.

Figures 5–8 show the influences of various parameters on the velocity profile in the z-direction. Generally, the effects of pressure gradient, slip parameter, Hall current parameter, Casson fluid parameter, magnetic field parameter, rotation parameter, the Reynolds number, and the Prandtl number are parabolic in nature. The velocity profile has a maximum value at the centerline and attains its minimum value at the channel walls. It is noteworthy to mention that an increase in the pressure gradient, slip parameter, Hall current parameter, Casson fluid parameter, magnetic field parameter and rotation parameter, as shown in Figs 5, 6 and 7, increases the velocity profiles, while the increase in the Reynolds number and the Prandtl number reduces the velocity profile, as shown in Fig. 8.

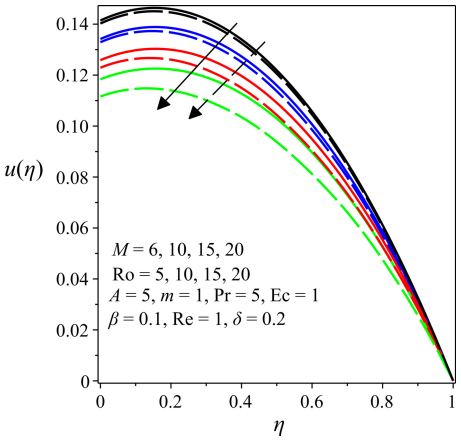

FIG. 4. Velocity profile with varied M and Ro.

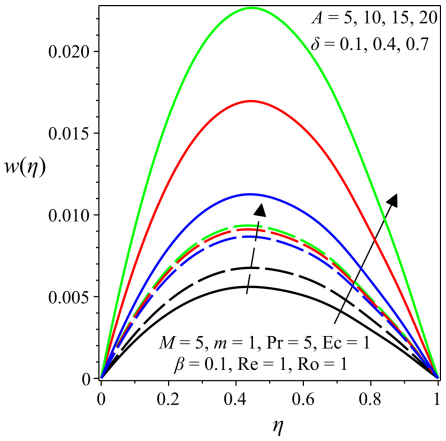

FIG. 5. Velocity profile in the z-direction with varied A and δ.

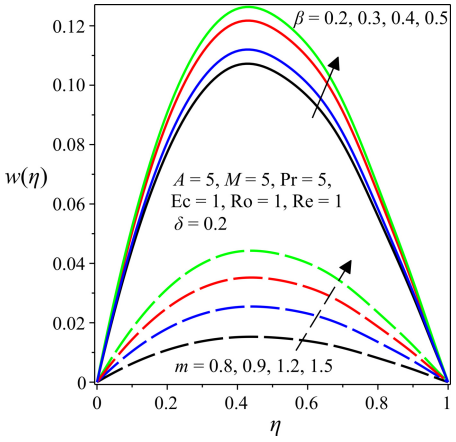

FIG. 6. Velocity profile in the z-direction with varied m and β.

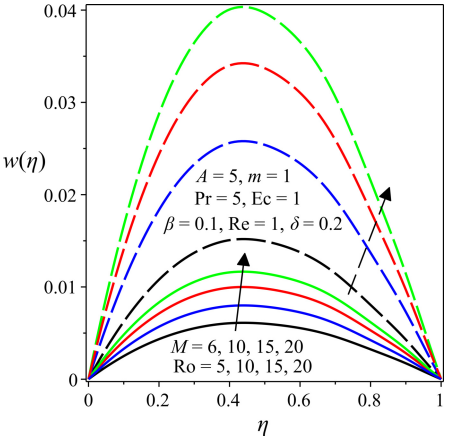

FIG. 7. Velocity profile in the z-direction with M and Ro.

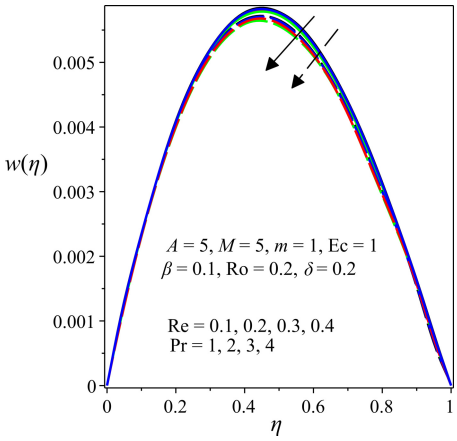

FIG. 8. Velocity profile in the z-direction with varied Re and Pr.

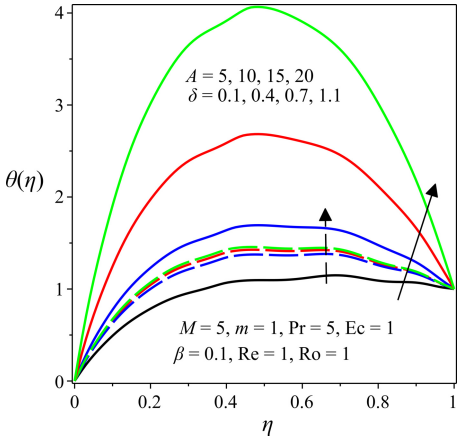

FIG. 9. Temperature profile with varied A and B.

The effects of various physical parameters on the temperature profile are shown in Figs 9–12. Figure 9 illustrates the effect of the pressure gradient on the temperature profile. The temperature profile rises with an increasing pressure gradient. This is attributed to the fact that an increase in pressure gradient with constant density leads to a rise in temperature. Similarly, an increase in the slip parameter has an indirect effect on the temperature profile. In Fig. 10, we can observe the effects of the Hall current parameter and the Casson fluid parameter on the temperature flow field. It is seen that temperature profile increases with increasing Hall current and Casson fluid parameters. The effect of the magnetic field parameter and rotation parameter on the temperature profile

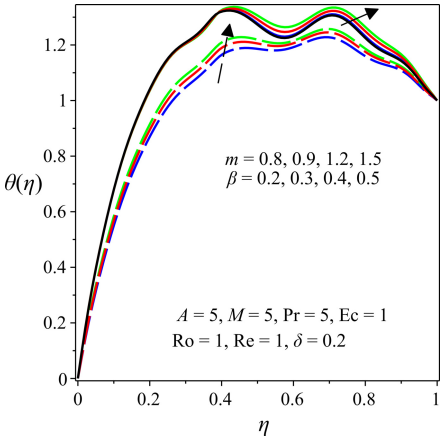

FIG. 10. Temperature profile with varied m and β.

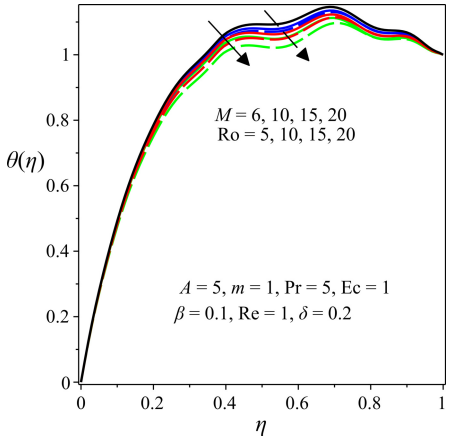

FIG. 11. Temperature profile with varied M and Ro.

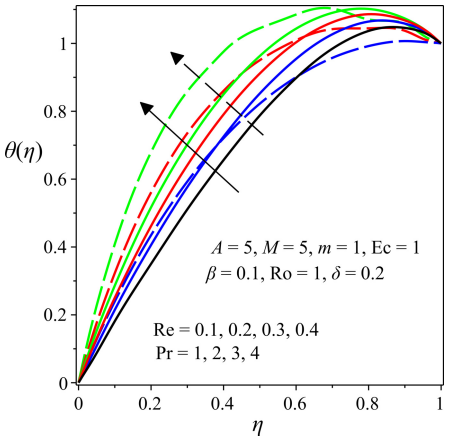

FIG. 12. Temperature profile with varied Re and Pr.

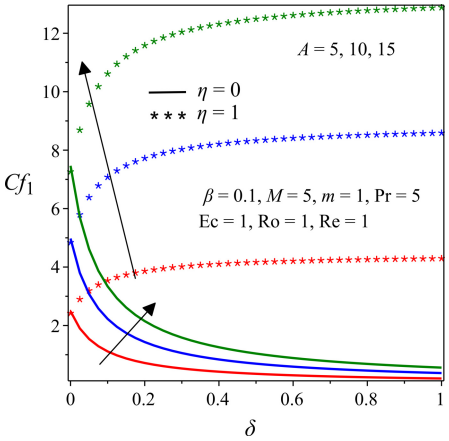

FIG. 13. Skin friction (Cf_1) with increasing A and B.

is shown in Fig. 11. It is observed that, as these parameters are increasing, the temperature profile decreases. This may be attributed to the fact that the surface boundary effect permits the effect of the magnetic field parameter. The effects of the Reynolds number and Prandtl number are displayed in Fig. 12. The temperature profile increases with increasing each of these parameters. This may be attributed to the fact that the surface boundary effect annuls the effect of the Reynolds and Prandtl numbers.

Figures 13–18 present the effects of some parameters on primary skin friction, secondary skin friction and the Nusselt number. Figure 13 shows the influences of the pressure gradient and slip parameter on the primary skin friction. It can be

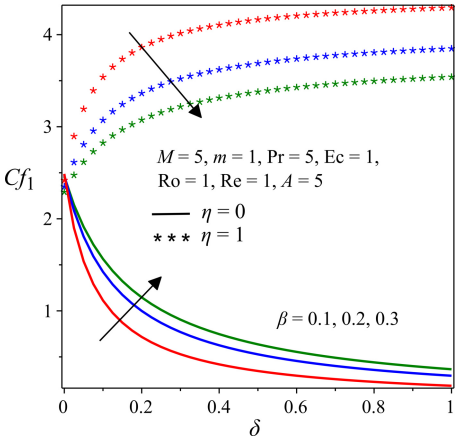

FIG. 14. Skin friction (Cf_1) with increasing β and δ.

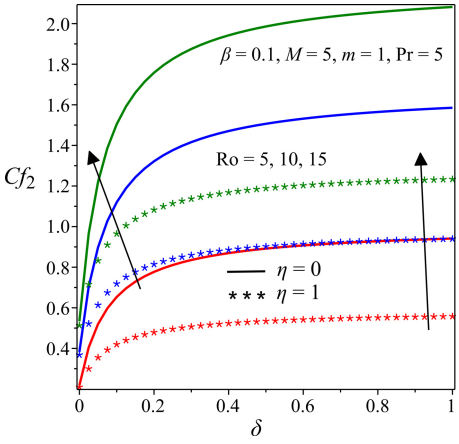

FIG. 15. Skin friction (Cf_2) with increasing Ro and δ.

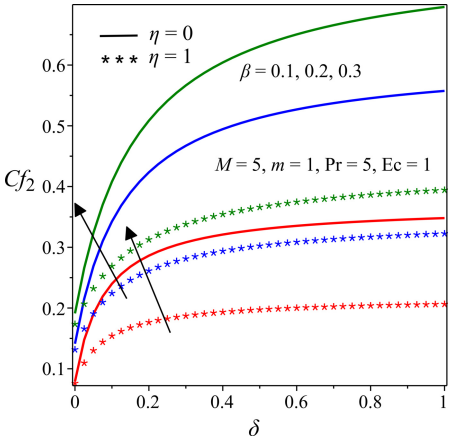

FIG. 16. Skin friction (Cf_2) with increasing β and δ.

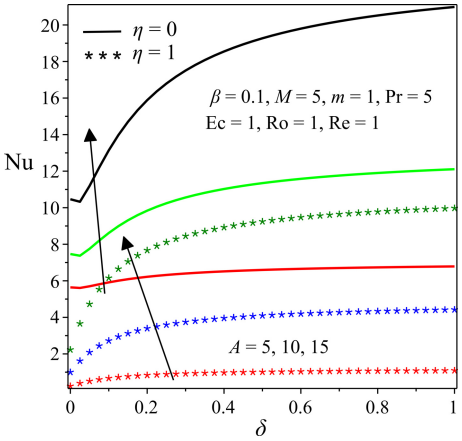

FIG. 17. Nusselt number with increasing A and δ.

seen that, as these parameters are increasing, the primary skin friction increases at the lower and upper walls, respectively. The Casson fluid and slip parameters influences on primary skin friction are depicted in Fig. 14. It is observed that the primary skin friction at the upper wall reduces while at the lower wall it increases with increasing Casson fluid and slip parameters. Figures 15 and 16 illustrate the impact of the rotation parameter, Casson fluid parameter and slip parameter on the secondary skin friction. We observed in these figures that the secondary skin friction increased at the upper and lower walls. Figures 17 and 18 illustrate the effects of the pressure gradient parameter, Casson fluid parameter and slip parameter on the Nusselt number. It is seen that an increase in these parameters

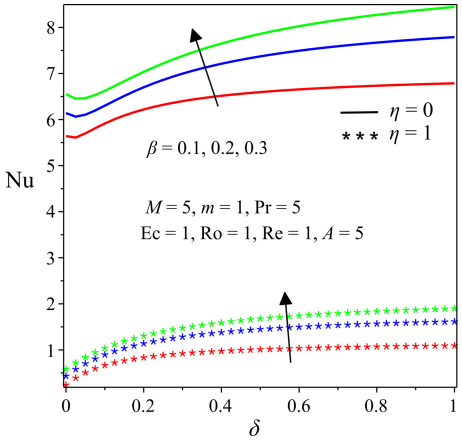

FIG. 18. Nusselt number with varied β and δ.

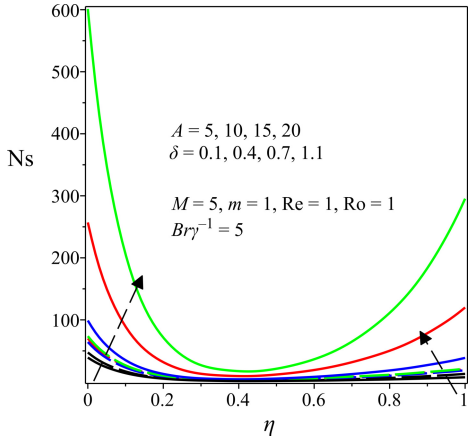

FIG. 19. Entropy profile with varied A and δ.

speeds up heat transfer. The boundary layer thickness at both walls was affected by the pressure gradient due to the momentum and energy equations.

Figures 19 and 20 show the impacts of the pressure gradient, slip parameter, Reynolds number and Prandtl number on the entropy generation profile. We observed from these figures that entropy rises with an increase in each of these parameters at the boundary layer region due to a more restrictive medium. Meanwhile, these parameters do not seem to show any effect along the centerline of the flow region because there is little or no restrictive medium.

The effects of the pressure gradient, slip parameter, Reynolds number and Prandtl number on the Bejan number are represented in Figs 21 and 22. As the slip parameter increases, we noticed a reduction in the Bejan number between

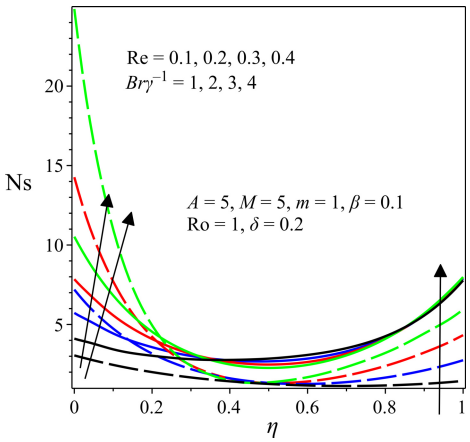

FIG. 20. Entropy profile with varied Re and $Br\gamma^{-1}$.

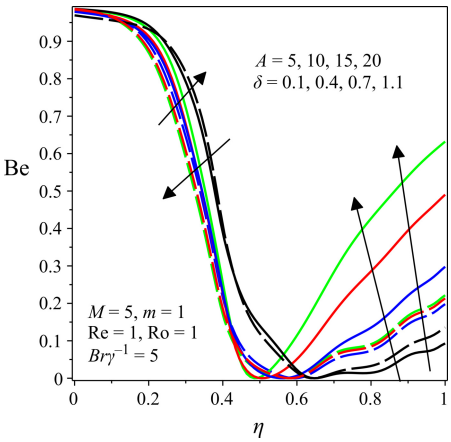

FIG. 21. Bejan number profile with varied A and δ.

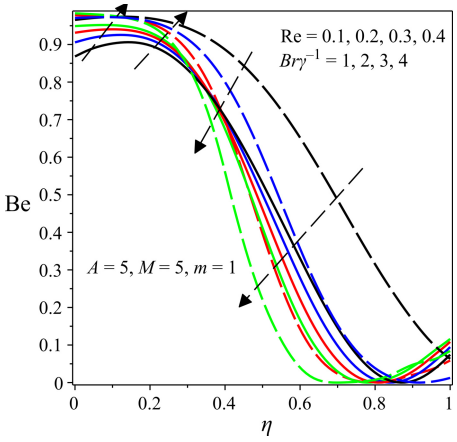

FIG. 22. Bejan profile with varied Re and $Br\gamma^{-1}$.

$\eta = 0$ and after that its increase. This means that the mutual effects of the fluid friction and magnetic field irreversibility dominate between $\eta = 0$ and $\eta \approx 0.5$ while thermodynamic irreversibility due to heat transfer dominates thereafter. An increase in the pressure gradient increases the Bejan number. This implies that the thermodynamic irreversibility due to heat transfer dominates as the pressure gradient is increasing. Figure 22 displays the influences of the Reynolds number and Prandtl number on the Bejan number. As the value of these parameters increases, we noticed a rise in the Bejan number up to $\eta \approx 0.3$ and the cross-flow at $\eta \approx 0.3$ and $\eta \approx 0.8$. The thermodynamic irreversibility due to heat transfer dominates from $\eta = 0.1$ to $\eta \approx 0.3$. The mutual effects of the fluid friction and magnetic field irreversibility dominate between $\eta \approx 0.3$ and $\eta \approx 0.8$.

4. Summary and conclusions

We carried out the thermodynamics analysis of a MHD Casson fluid flow through a rotating permeable microchannel with slip and Hall effects. Some of the thermophysical parameters‘ values were fixed. Our results revealed the following:

- The increase in the Casson fluid parameter and Hall current parameter increased the fluid velocity profiles.
- Increasing slip and Casson fluid parameters increase the temperature in the centerline channel.
- It was also found that both fluid rotation and velocity slip escalate the entropy generation rate.
- While fluid injection at the lower wall boosted the entropy production, fluid suction at the upper wall lessened it.

Finally, we would like to emphasize that the above model and its results can only be applied to the microchannel flow-related problem. This can be viewed as the limitation of the present study. Moreover, our results will undoubtedly augment the design and efficient operation of micro-cooling devices, micro-heat exchangers, micropumps and micro-mixing technologies.

References

1. Casson N., A flow equation for pigment oil-suspensions of the printing ink type, *Rheology of Disperse Systems*, C.C. Mill [Ed.], pp. 84–104, Pergamon Press, London, 1959.

2. Gireesha B.J., Archana M., Prasannakumara B.C., Reddy Gorla R.S., Makinde O.D., MHD three dimensional double-diffusive flow of Casson nanofluid with buoyancy forces and nonlinear thermal radiation over a stretching surface, *International Journal of Numerical Methods for Heat & Fluid Flow*, **27**(12): 2858–2878, 2017, doi: 10.1108/HFF-01-2017-0022.

3. Zaib A., Rashidi M., Chamkha A.J., Bhattacharyya K., Numerical solution of second law analysis for MHD Casson nanofluid past a wedge with activation energy and binary chemical reaction, *International Journal of Numerical Methods for Heat & Fluid Flow*, **27**(12): 2816–2834, 2017, doi: 10.1108/HFF-02-2017-0063.

4. Gupta S., Sharma K., Numerical simulation for the magnetohydrodynamic three-dimensional flow of Casson nanofluid with convective boundary conditions and thermal radiation, *Engineering Computations*, **34**(8): 2698–2722, 2017, doi: 10.1108/EC-02-2017-0064.

5. Durairaj M., Ramahandran S., Mehdi R.M., Heat generating/absorbing and chemically reacting Casson fluid flow over a vertical cone and flat plate saturated with a non-Darcy porous medium, *International Journal of Numerical Methods for Heat & Fluid Flow*, **27**(1): 156–173, 2017, doi: 10.1108/HFF-08-2015-0318.

6. Hymavathi T., Sridhar W., Numerical solution to mass transfer in MHD flow of Casson fluid with suction and chemical reaction, *International Journal of Chemical Sciences*, **14**(4): 2183–2197, 2016.

7. Hussanan A., Salleh M.Z., Khan I., Tahar R.M., Heat transfer in magnetohydrodynamic flow of a Casson fluid with porous medium and Newtonian heating, *Journal of Nanofluids*, **6**(4): 784-793, 2017, doi: 10.1166/jon.2017.1359.

8. Rawi N.A., Ilias M.R., Lim Y.J., Isa Z.M., Shafie S., Unsteady mixed convection flow of Casson fluid past an inclined stretching sheet in the presence of nanoparticles, *Journal of Physics: Conference Series*, **890**: 012048, 2017, doi: 10.1088/1742-6596/890/1/012048.

9. Eegunjobi A.S., Makinde O.D., Inherent irreversibility in a variable viscosity Hartmann flow through a rotating permeable channel with Hall effects, *Defect and Diffusion Forum*, **377**: 180–188, 2017, doi: 10.4028/www.scientific.net/ddf.377.180.

10. Singh J.K., Seth G.S., Begum S.G., Unsteady MHD natural convection flow of a rotating viscoelastic fluid over an infinite vertical porous plate due to oscillating free-stream, *Multidiscipline Modeling in Materials and Structures*, **14**(2): 236–260, 2018, doi: 10.1108/MMMS-06-2017-0054.

11. Rashidi M.M., Erfani E., Analytical method for solving steady MHD convective and slip flow due to a rotating disk with viscous dissipation and Ohmic heating, *Engineering Computations*, **29**(6): 562–579, 2012, doi: 10.1108/02644401211246283.

12. Papa F., Vaidyanathan K., Keith T.G., DeWitt.J., Numerical computations of flow in rotating ducts with strong curvature, *International Journal of Numerical Methods for Heat & Fluid Flow*, **10**(5): 541–557, 2000, doi: 10.1108/09615530010338213.

13. Arikoglu A., Ozkol I., On the MHD and slip flow over a rotating disk with heat transfer, *International Journal of Numerical Methods for Heat & Fluid Flow*, **16**(2): 172–184, 2006, doi: 10.1108/09615530610644253.

Received September 5, 2018; accepted version May 28, 2020.
